ESC European Society of Cardiology

Cardiovascular Research (2019) **115**, 230–242
doi:10.1093/cvr/cvy206

Long non-coding RNA H19 regulates endothelial cell aging via inhibition of STAT3 signalling

Patrick Hofmann[1,2], Janina Sommer[1], Kosta Theodorou[1], Luisa Kirchhof[1], Ariane Fischer[1], Yuhuang Li[3,4], Ljubica Perisic[5], Ulf Hedin[5], Lars Maegdefessel[3,4,6], Stefanie Dimmeler[1,2], and Reinier A. Boon[1,2,7]*

[1]Institute of Cardiovascular Regeneration, Centre of Molecular Medicine, Goethe-University, Theodor Stern Kai 7, 60590 Frankfurt, Germany; [2]German Center for Cardiovascular Research DZHK, Partner Site Frankfurt Rhine-Main, Berlin, Germany; [3]Department of Vascular and Endovascular Surgery, Technical University Munich, Munich, Germany; [4]German Center for Cardiovascular Research DZHK, Partner Site Munich, Berlin, Germany; [5]Department of Molecular Medicine and Surgery, Karolinska Institute, Stockholm, Sweden; [6]Department of Medicine, Karolinska Institute, Stockholm, Sweden; and [7]Department of Physiology, Amsterdam Cardiovascular Sciences, VU University Medical Center, Amsterdam, The Netherlands

Received 24 July 2018; revised 6 August 2018; editorial decision 9 August 2018; accepted 10 August 2018; online publish-ahead-of-print 13 August 2018

Time for primary review: 8 days

Aims Long non-coding RNAs (lncRNAs) have been shown to regulate numerous processes in the human genome, but the function of these transcripts in vascular aging is largely unknown. We aim to characterize the expression of lncRNAs in endothelial aging and analyse the function of the highly conserved lncRNA H19.

Methods and results H19 was downregulated in endothelium of aged mice. In human, atherosclerotic plaques H19 was mainly expressed by endothelial cells and H19 was significantly reduced in comparison to healthy carotid artery biopsies. Loss of H19 led to an upregulation of p16 and p21, reduced proliferation and increased senescence *in vitro*. Depletion of H19 in aortic rings of young mice inhibited sprouting capacity. We generated endothelial-specific inducible H19 deficient mice ($H19^{iEC\text{-}KO}$), resulting in increased systolic blood pressure compared with control littermates (Ctrl). These $H19^{iEC\text{-}KO}$ and Ctrl mice were subjected to hindlimb ischaemia, which showed reduced capillary density in $H19^{iEC\text{-}KO}$ mice. Mechanistically, exon array analysis revealed an involvement of H19 in IL-6 signalling. Accordingly, intercellular adhesion molecule 1 and vascular cell adhesion molecule 1 were upregulated upon H19 depletion. A luciferase reporter screen for differential transcription factor activity revealed STAT3 as being induced upon H19 depletion and repressed after H19 overexpression. Furthermore, depletion of H19 increased the phosphorylation of STAT3 at TYR705 and pharmacological inhibition of STAT3 activation abolished the effects of H19 silencing on p21 and vascular cell adhesion molecule 1 expression as well as proliferation.

Conclusion These data reveal a pivotal role for the lncRNA H19 in controlling endothelial cell aging.

Keywords Endothelium • Inflammation • Senescence • Non-coding RNA

1. Introduction

Cardiovascular disease is the leading cause of death worldwide.[1] Aging is a major independent risk factor for cardiovascular disease and is accompanied by a structural and functional decline in many organs. Aging of the vasculature is characterized by thickened intima, increased arterial stiffness, endothelial dysfunction, and chronic vascular inflammation.[2] On the cellular level, aging leads to cellular senescence and increased inflammatory activation. The onset of senescence is usually due to telomere shortening and/or DNA damage response pathways.[3] Senescence is established by two major pathways, the p53/p21 and $p16^{INK4a}$/pRB pathways, and has a detrimental effect in many age-related diseases.[4–6] Endothelial cell senescence is associated with reduced synthesis of nitric oxide and endothelial dysfunction,[7,8] which is a risk factor for the development of atherosclerosis.[9] Senescent cells secret many pro-inflammatory cytokines and chemokines, including IL-6 and IL-8 and can

* Corresponding author. Tel: +4969630185397; fax: +4969630185398, E-mail: boon@med.uni-frankfurt.de, r.boon@vumc.nl

thus induce inflammation in the surrounding tissue.[10–12] Increased inflammatory signalling on the other side was shown to promote senescence and to shorten lifespan in mice,[13] while the depletion of p16^{ink4a}-positive cells *in vivo* was shown to significantly increase lifespan in mice.[14] One of the major causes of age-related diseases seems to be vascular decline,[15] and interestingly, induction of angiogenesis in aged mice rescued detrimental effects of aging, showing that some effects of aging can be reversed.[16]

Atherosclerotic lesion formation initiates at sites of endothelial inflammation, where endothelial cells express cell surface adhesion molecules. Senescent ECs are present within atherosclerotic plaques[17] and vascular smooth muscle cell senescence was shown to promote the formation of atherosclerotic plaques.[18–20] Furthermore, inflammatory signalling in ECs induces IL-6 secretion, along with inflammatory adhesion molecules on the cell surface[21] and IL-6 plays a central role in propagating the inflammatory response in atherosclerosis development.[22] IL-6 activates signal transducer and activator of transcription 3 (STAT3) by inducing STAT3 phosphorylation at TYR705 by janus kinase 2 (JAK2). STAT3 inhibition was shown to promote satellite cell expansion and tissue repair in aged mice.[23] Furthermore, STAT3 induces p21 expression via transcriptional activation of FOXP3 and by direct binding in the p21 gene promoter region.[24,25] It was furthermore shown to upregulate the expression of intercellular adhesion molecule 1 (ICAM-1) in human hepatocellular carcinoma cells and in endothelial cells.[26,27] In addition, STAT3 induced IL-6 levels by direct binding to the IL-6 promoter region in a protein kinase C ϵ dependent manner.[28,29]

Long non-coding RNAs (lncRNAs) are RNAs that are not translated into protein and are more than 200 nucleotides in length. The database lncipedia currently lists 111 685 annotated lncRNAs of different biotypes in humans.[30] LncRNAs have been shown to play important roles in the cardiovascular system.[31] For example, the depletion of MALAT1 in ECs inhibits vascular growth *in vivo* and *in vitro*.[32] H19 was one of the first known lncRNAs and is located on 11p15 in humans.[33,34] The locus encoding H19 is evolutionary conserved in mammals, is located upstream of insulin growth factor 2 (IGF2) and is paternally imprinted.[35] H19 is upregulated again during tissue regeneration, carcinogenesis and upon hypoxia.[36–39] In a recent study, H19 was shown to be upregulated by treatment with prostacyclin producing human mesenchymal stem cells and to promote cell survival and proliferation in a hindlimb ischaemia model.[40] Another study highlights the role of H19 in calcific aortic valve disease, where it prevented the recruitment of p53 to the NOTCH1 promoter.[41] However, until now, H19 has not been described to be involved in aging of the cardiovascular system.

Here, we show that H19 is expressed in the adult endothelium and is decreased during aging. H19 depletion in endothelial cells results in premature senescence. Furthermore, H19 loss-of-function induces inflammatory signalling *via* the STAT3 signalling pathway. Inhibition or endothelial-specific genetic deletion of H19 reduces endothelial cell function and overexpression of H19 ameliorates endothelial function in aged aortas. These results show a central role of H19 in reducing endothelial cell aging.

2. Methods

2.1 Cell culture

Human umbilical vein endothelial cells (HUVECs) were purchased from Lonza (Lots p997 and p1028) and cultured in endothelial basal medium (EBM; Lonza), supplemented with EGM SingleQuots (Lonza) and 10% foetal calf serum (FCS; Invitrogen. San Diego, CA, USA). Human coronary artery endothelial cells were purchased from Promocell and cultured in endothelial growth medium MV (Promocell). Primary cells were used between Passage 2 and 4 for experiments. HeLa cells were cultured in Dulbecco's Modified Eagle Medium (DMEM) with 10% FCS, D-Glucose, Pyruvate, Penicillin/streptomycin, and minimum essential media non-essential amino acid mix (Sigma Aldrich); Hek293T cells were cultured in DMEM with 10% heat inactivated FCS, D-Glucose, Pyruvate, and Penicillin/streptomycin. Cells were cultured at 37°C with 5% CO_2. Cell numbers were determined with a Nucleocounter NC-2000 (Chemometec A/S). HUVECs were stimulated with 100 ng/mL IL-6 (Peprotech) and sIL-6Rα (Peprotech) each in EBM for 10 min (for pSTAT3 Y705 western blots) or 4 h before cell lysates were prepared. A 20 μM Cryptotanshinone (CPT; Sigma Aldrich) in Dimethyl sulfoxide (DMSO) was added to cell culture medium 1 h prior to addition of IL-6 and sIL-6Rα. Equal volumes of DMSO were used as controls for CPT experiments.

2.2 BiKe

Patients undergoing surgery for symptomatic or asymptomatic, high-grade (>50% NASCET[42]) carotid stenosis at the Department of Vascular Surgery, Karolinska University Hospital, Stockholm, Sweden, were enrolled in the Biobank of Karolinska Endarterectomies (BiKE) study. Symptoms of plaque instability were defined as transitory ischaemic attack, minor stroke, and *amaurosis fugax*. Patients without qualifying symptoms within 6 months prior to surgery were categorized as asymptomatic and indication for carotid endarterectomy based on results from the Asymptomatic Carotid Surgery Trial (ACST).[43] Carotid endarterectomies (carotid plaques) were collected at surgery (totally 127) and normal artery controls were obtained from nine macroscopically disease-free iliac arteries and one aorta from organ donors without any history of cardiovascular disease (totally 10). All samples were collected with informed consent from patients or organ donors guardians. All human studies were approved by the regional Ethics Committee. The BiKE study follows the principles outlined in the declaration of Helsinki. The BiKE study cohort demographics, details of sample collection, processing, and large-scale profiling analyses were previously extensively described.[44,45] The microarray dataset is available from Gene Expression Omnibus (GSE21545).

2.3 *In situ* hybridization

For *in situ* hybridization on human tissue samples from the Munich Vascular Biobank,[46] an Exiqon miRCURY LNA Digoxigenin (DIG)-labelled probe (5'-3' sequence:/5DigN/ATACAGCGTCACCAAG TCCA/3Dig_N/) was used with the accompanying kit and according to the manufacturer's protocol for paraffin-embedded sections (Exiqon, Vedbaek, Denmark). In brief, tissue sections were deparaffinized (formalin-fixed paraffin-embedded) and rehydrated. Nucleases were inactivated with Proteinase K, followed by a 2 h hybridization interval at 56°C. Slides were washed in saline-sodium citrate buffers with subsequent DIG detection methods.

2.4 Human tissue morphology analysis and immunohistochemistry

Human carotid arterial plaque material was sampled during carotid-endarterectomy, fixed for 48 h in 2% zinc-paraformaldehyde at room temperature, paraffin-embedded and cut into 5 μm thick slides. Per carotid plaque specimen, four slides were stained with haematoxylin and

eosin (HE) as well as van Gieson's staining. Plaques were classified as ruptured or stable according to their histomorphologic AHA classification[47] and critical fibrous cap thickness as described by Redgrave *et al.*[48] Per group (ruptured or stable), five representative whole plaque transverse sections from three different plaques were selected for staining. Control carotid arteries were obtained from deceased organ donors without any reported history of advanced or severe cardiovascular disease.

For immunohistochemistry a standard biotin-avidin-immunoperoxidase method with a monoclonal mouse anti-human antibody from Agilent (Santa Clara, CA, USA) for CD31 was utilized.

2.5 qRT-PCR

Total RNA from cultured cells and mouse tissues was isolated with Qiagen miRNeasy kit (Qiagen, Hilden, Germany) according to the manufacturer's protocol. Nuclear and cytoplasmic RNA was isolated as previously described.[49] For Real Time Quantitative PCR (qRT-PCR) analysis, 100–1000 ng total RNA was reverse transcribed using random hexamer primers (Thermo Fisher Scientific) and either MulV or Superscript reverse transcriptase (Applied Biosystems). qRT-PCR was done with Fast SYBR Green Master Mix (Applied Biosystems) in Applied Biosystems StepOne Plus or Viia7 devices. Ribosomal protein, large, P0 (RPLP0) or glyceraldehyde-3-phosphate dehydrogenase (GAPDH) were used for normalization. Gene expression analysis was done using the $2^{-\Delta CT}$ method. Primer sequences can be found in Supplementary material online, *Table S1B*.

2.6 GapmeRs/siRNAs

Cultured cells were transfected at 60–70% confluence with 66.6-nM siRNAs (Qiagen, Hilden, Germany) using Lipofectamine RNAiMax (Life Technologies) according to the manufacturer's protocol in serum reduced OptiMEM medium (Life Technologies). A siRNA against firefly luciferase (Sigma Aldrich, St. Louis, MO, USA) was used in the same concentrations. The medium was changed after 4 h of transfection to full growth medium. Sequences of the siRNAs can be found in Supplementary material online, *Table S1C*.

2.7 Lentivirus

Long-term overexpression and suppression of KLF2 was done according to Dekker *et al.*[50] Human H19 (ENST00000412788) full length cDNA was cloned into pLenti4/v5 (Life Technologies). Lentivirus stocks were produced in Hek293T cells using pCMVΔR8.91 as packaging plasmid and pMD2.G (Addgene #12259) as vesicular stomatitis virus G glycoprotein envelope expressing plasmid.[51] Empty vectors were used as control. Transduction was done for 24 h.

2.8 Western blot analysis

HUVECs were lysed in Radioimmunoprecipitation assay (RIPA) buffer (Sigma Aldrich) for 15 min on ice. After centrifugation with 10 000 × *g*, protein content was analysed with Pierce BCA Protein Assay Kit (Thermo Scientific). Equal amounts of protein were loaded on Sodium dodecyl sulfate gels and blotted on nitrocellulose membranes. Tubulin α or Actin was used as loading controls. Antibodies are listed in Supplementary material online, *Table S1A*.

2.9 Proliferation assay

Cells were incubated with 10 mM BrdU for 45 min (HUVECs) or 16 h (hCoAECs) and analysis was performed using the BrdU Flow Kit (BD Pharmingen) according to the manufacturer's protocol. Cells were stained with anti-BrdU-V450 or anti-BrdU-FITC for 20 min and 7-Aminoactinomycin D for 10 min and analysed using a FACS Canto II device (BD Bioscience).

2.10 Senescence associated β-Galactosidase staining

Senescence associated β-Galactosidase activity was analysed with the Senescence Associated β-Galactosidase Staining kit (Cell Signalling Technologies #9860). Images were taken with 5× magnification with a Zeiss Axiovert 100 and the number of total cells, as well as the number of stained cells was determined in five images per condition and experiment.

2.11 Monocyte adhesion assay

Monocytes were isolated from fresh buffy coats. HUVECs were transfected 48 h prior to the assay and transferred to gelatin-coated 96-well plates and stimulated with IL-6 and sIL-6Rα 24 h prior to the assay. In 6 × 10^5 2', 7'-Bis-(2-Carboxyethyl)-5-(and-6)-Carboxyfluorescein, Acetoxylmethyl Ester (BCECF, Thermo Fisher Scientific)-stained monocytes were added to the HUVEC monolayer and plates were incubated 30 min at 37°C, 5% CO_2. Vascular cell adhesion molecule 1 (VCAM-1) was blocked with 30 µg/mL anti-human VCAM-1 (BBA5, R&D Systems). Baseline fluorescence was measured in an ELISA reader, and wells were washed six times in total with Hank's balanced salt solution and fluorescence was measured again.

2.12 Microarrays

Microarray analysis of HUVEC total RNA was performed on the human GeneChip Gene 2.0 ST platform (Affymetrix, Santa Clara, CA, USA), as previously described.[52] The Database for Annotation, Visualization and Integrated Discovery (DAVID) bioinformatics resources were utilized for pathway analysis of gene ontology terms.

2.13 Aortic rings

Aortic rings were prepared as previously described.[53] For overexpression, the same lentiviral stocks and concentrations as for cultured cells were used. Transduction was done for 24 h in OptiMEM (Life Technologies). Depletion of H19 was done with a mouse specific LNA GapmeR against H19 or GapmeR control A (Exiqon, Vedbaek, Denmark) for 24 h in OptiMEM with Lipofectamine RNAiMax (Life Technologies). Mosaic pictures were taken with a Zeiss Axiovert microscope with 5× magnification. The cumulative sprout length was determined with Zeiss Axiovision software. LNA GapmeR sequences can be found in Supplementary material online, *Table S1C*.

2.14 RNA immunoprecipitation

Cells were crosslinked with 50 mJ/cm^2 UV light and lysed with total lysis buffer (50 mmol/l Tris-HCl pH8, 150 mmol/l NaCl, 0.5% NP-40, and protease inhibitors). The lysates were cleared by centrifugation at 10 000 × *g* and incubated with protein G magnetic beads (Life Technologies) coated with antibodies listed in Supplementary material online, *Table S1A* for 4 h at 4°C, and then washed with lysis buffer with 0.05% NP40. RNA was recovered after protein digestion with Proteinase K and nucleic acids isolated by phenol/chlorophorm/isoamyl extraction and analysed by qRT-PCR.

2.15 ELISA

The expression of human IL-6 was determined with human IL-6 enzyme-linked immunosorbent assay (ELISA) kit (Invitrogen) according to the manufacturer's instructions. HUVECs were lysed with RIPA buffer and the protein content was analysed with Pierce BCA Protein Assay kit (Thermo Scientific). A total of 10 µg protein was used per sample for the ELISA and signals were analysed with a Promega GloMax Multi+ device.

2.16 Flow cytometry

Cells were stimulated with 100 ng/mL IL-6 (Peprotech) and sIL-6Rα (Peprotech) overnight. Cells were detached with 1 mM EDTA solution, stained with anti-ICAM-1 (Biolegend), and anti-VCAM-1 (Biolegend) antibodies, fixed with 4% paraformaldehyde and analysed using a FACS Canto II device (BD Bioscience).

2.17 Animal experiments

All mice experiments were carried out in accordance with the principles of laboratory animal care as well as according to the German national laws and the guidelines from Directive 2010/63/EU of the European Parliament on the protection of animals used for scientific purposes. The studies have been approved by the local ethics committee (Regierungspräsidium Darmstadt, Hessen). Cdh5(PAC)-CreERT2-H19 flox mice on a C57Bl6/J background were injected intraperitoneally with tamoxifen seven times during 3 weeks prior to surgery, organ harvest, or blood pressure analysis. Cdh5(PAC)$^{CreERT2/+}$; H19$^{fl/fl}$ (referred to as H19$^{iEC\text{-}KO}$) and Cre-negative H19$^{fl/fl}$ and H19$^{fl/+}$ (referred to as Ctrl) mice were used. The 10 µm sections of the frozen soleus muscle were used for morphological analysis. Hind-limb ischaemia and subsequent laser-Doppler perfusion measurement and assessment of capillary density were performed as described.[54] Briefly, animals were anaesthetized with isoflurane and analgesia was carried out with Buprenorphin (Temgesic®, 0.1 mg/kg body weight every 12 h for 3 days, s.c.) and Carprofen (Rimadyl®, 5 mg/kg body weight every 24 h for 6 days, s.c.). Animals were sacrificed by cervical dislocation. Animal health was evaluated daily. Genders were 3×♀ and 2×♂ for Ctrl and 1×♀ and 4×♂ for endothelial-specific inducible H19 deficient mice (H19$^{iEC\text{-}KO}$). The mice were between 16 and 17 weeks old at the start of the experiment. For blood pressure analysis, genders were 2×♀ and 3×♂ for both groups. The mice were 12 weeks old at the start of the experiment. Blood pressure was measured daily during two weeks with the Visitech-Systems BP-2000 tail cuff system. Fifteen measurements were done per day and the last 10 were used for analysis. H19 flox and Cdh5(PAC)-CreERT2 mice were kindly provided by Karl Pfeifer (NIH, Bethesda, MD, USA) and Ralf Adams (MPI, Münster, Germany), respectively. Antibodies and reagents are listed in Supplementary material online, *Table S1A*.

2.18 Statistical analysis

Data are expressed as mean ± standard error of the mean (SEM). GraphPad Prism 5 and 7 were used for statistical analysis. Data were tested for Gaussian distribution with the Kolmogorov–Smirnov test (with Dallal-Wilkinson–Lilliefor *P*-value) and paired or unpaired Student's *t*-test or Mann–Whitney test was performed when comparing two groups. Analysis of variance (ANOVA) followed by Tukey's post-test was performed for multiple comparisons. Outliers within a group were detected with a Grubbs' outlier test and significant outliers ($P < 0.05$) were excluded from the analysis. Statistical significance was depicted as follows: $^{*}P < 0.05$, $^{**}P < 0.01$, $^{***}P < 0.001$, n.s. = not statistically significant.

3. Results

3.1 H19 is expressed in the endothelium and repressed by aging

To assess aging-induced lncRNA expression regulation in the cardiovascular system, previously published microarray data of organs from young (8 weeks) and aged (18 months) mice were analysed.[52,55] The lncRNA H19 was repressed by aging especially in lung endothelial cells of aged mice compared with young mice, but was not affected in other tissues (*Figure 1A*). Further dissection of the aorta in aortic intima and aortic media/adventitia in a second cohort of mice and measurement of expression by qRT-PCR confirmed that H19 was repressed by aging in endothelial cells selectively (*Figure 1B*). Analysis of human atherosclerotic plaques from carotid arteries revealed a repression of H19 expression compared to healthy arteries (*Figure 1C*). *In situ* hybridization in healthy carotid arteries revealed a colocalization of H19 with CD31, indicating that H19 is mainly expressed in the endothelium of healthy arteries (*Figure 1D*). Luminal endothelial cells from atherosclerotic plaques in carotid arteries did not express H19 but endothelial cells from intraplaque blood vessels showed H19 expression (*Figure 1D*). The two hallmarks of vascular aging are reduced proliferative capacity (and concomitant increase in senescence) and inflammatory activation. To assess if H19 contributes to either of these two features of aging, we first analysed the role of H19 in proliferation. siRNA-mediated depletion of H19 in HUVECs led to a significant reduction of cells in S- and G2/M-phase, while cells accumulated in G0/G1 phase (*Figure 2A* and Supplementary material online, *Figure S1A*). The same effect was observed in primary human coronary artery ECs (hCoAEC) (Supplementary material online, *Figure S1B*). An accumulation of cells in G0/G1 phase is an indication for cellular senescence and indeed, silencing of H19 increased the number of acidic β-galactosidase positive HUVECs and hCoAECs, which is a marker of cellular senescence (*Figure 2B and C*). In addition, upon silencing of H19, an upregulation of the cyclin-dependent kinase inhibitors p16 and p21 was observed (*Figure 2D* and *E*; Supplementary material online, *Figure S1C*). In concordance, lentivirus-mediated overexpression of H19 tended to reduce p16 and p21 expression (Supplementary material online, *Figure S1D* and *E*). Taken together, these results show that H19 inhibits senescence and promotes proliferation in endothelial cells.

3.2 H19 depletion impairs endothelial cell function *in vivo*

Endothelial cells from aged individuals exhibit less angiogenic activity *in vitro*.[56] To assess whether reduction in H19 contributes to endothelial cell functional decline during aging *in vivo*, an *ex vivo* aortic ring assay with young and aged mice was performed. The sprouting capacity of ECs from young (2 months) and aged (20 months) mice was analysed and in addition to that, H19 was depleted in aortic rings of young animals with LNA GapmeRs and human H19 was overexpressed in aortic rings of aged animals with lentivirus. In line with the data above (*Figure 1*), the expression of H19 was reduced in aortic rings of aged mice compared to young animals by nearly 50% (*Figure 3A*). Accordingly, the capacity of ECs to form sprouts was significantly decreased with aging (*Figure 3B and C*). Depletion of H19 with LNA GapmeRs in aortic rings of young animals led to a decrease of H19 RNA levels of roughly 50% compared with control treated aortic rings, comparable to the aging-mediated reduction (*Figure 3A*). Sprouting capacity was significantly reduced upon silencing of H19 to a similar extent as aging-mediated reduction of outgrowth. Moreover, overexpression of human H19 in aortic rings of aged animals

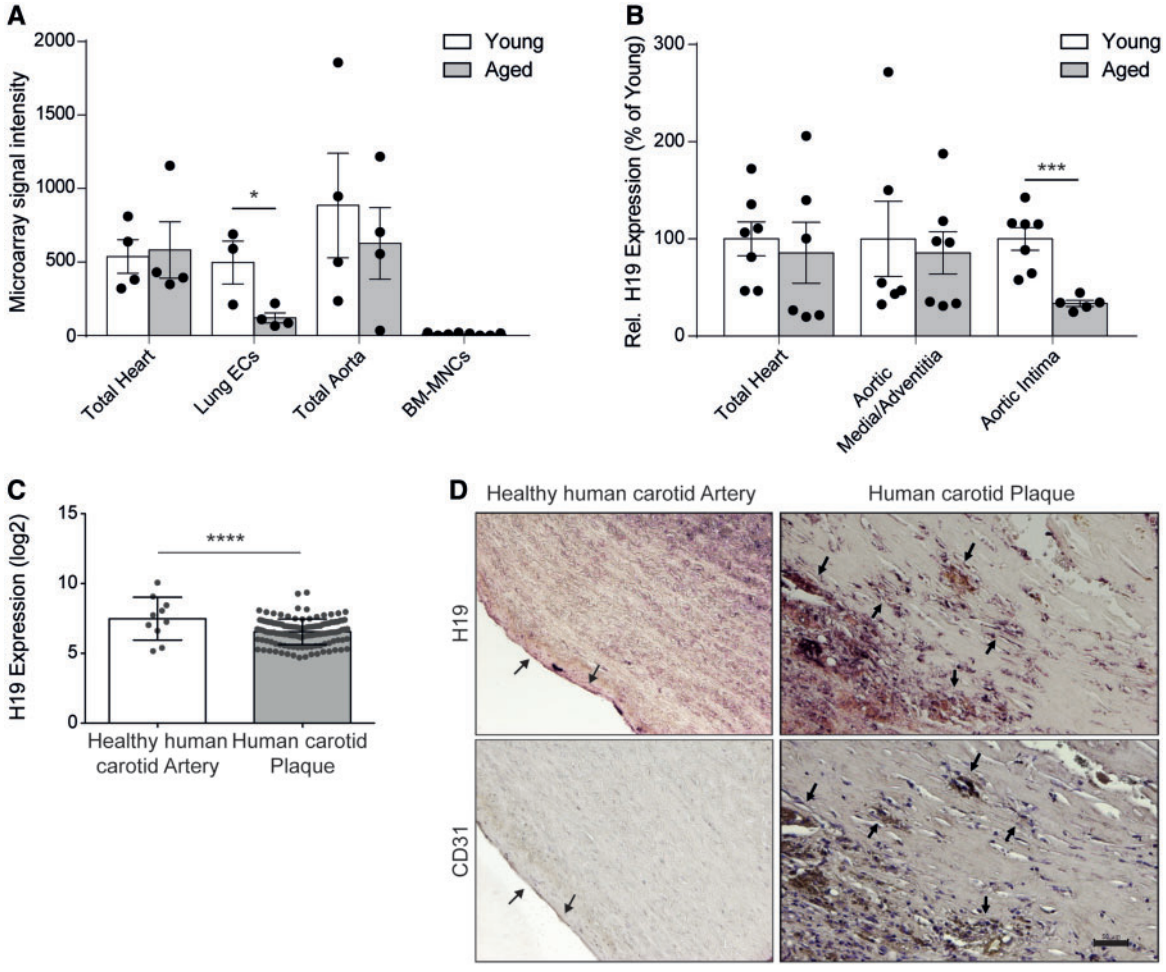

Figure 1 The lncRNA H19 is repressed with age and is mainly localized in the endothelium of blood vessels. (*A*) Differentially expressed transcripts with age were identified in a microarray screen of different mouse tissues from young (6 weeks, white bars) and aged (18 months, grey bars) mice. Microarray intensities corresponding to H19 levels are depicted. Results are represented as mean ± SEM from four mice per group. Unpaired *t*-test was used to determine statistical significance. (*B*) The same tissues as in *A* were isolated in a separate experiment, and the aortic intima was separated from the media/adventitia of the aorta. H19 was analysed by qRT-PCR. Results are represented as mean ± SEM from 5 to 7 mice per group. Unpaired *t*-test was used to determine statistical significance. (*C*) H19 expression was analysed in human tissue samples of healthy iliac arteries ($n = 9$) and healthy aorta ($n = 1$) and advanced carotid plaques ($n = 127$). Results are represented as mean ± SD. Unpaired *t*-test was used to determine statistical significance. (*D*) Localization of H19 in un-diseased human arteries and atherosclerotic lesions was analysed by *in situ* hybridization. An antibody against CD31 was used to visualize endothelial cells. Arrows indicate colocalization of H19 and CD31 staining. The scale bar denotes 50 μm; $^{*}P < 0.05$, $^{***}P < 0.001$, and $^{****}P < 0.0001$.

led to a trend towards the rescue of the aged phenotype and to cumulative sprout lengths comparable to those of young animals (*Figure 3B and C*; Supplementary material online, *Figure S1F*). To further substantiate this phenotype, aortas from $H19^{iEC\text{-}KO}$ were analysed for their angiogenic capacity in an aortic ring assay. Tamoxifen administration led to the almost complete deletion of H19 in ECs of $H19^{iEC\text{-}KO}$ mice (Supplementary material online, *Figure S1G*). EC sprouting was not significantly altered, but the proportion of aortic rings that did not form outgrowths at all was significantly higher in the $H19^{iEC\text{-}KO}$ group compared to Ctrl (*Figure 3D* and Supplementary material online, *Figure S1H*). To further analyse, the role of H19 *in vivo*, $H19^{iEC\text{-}KO}$ mice were subjected to hindlimb ischaemia. The analysis of capillary density in the ischaemic leg revealed significantly less capillaries in $H19^{iEC\text{-}KO}$ mice compared with Ctrl littermates, which is in line with the findings from the aortic ring assay (*Figure 3E*). Since increased blood pressure is another characteristic of cardiovascular aging,[2] we next measured blood pressure in these mice. While the diastolic blood pressure was not changed, $H19^{iEC\text{-}KO}$ mice showed an increase in systolic blood pressure compared with Ctrl littermates upon EC-specific deletion of H19 (Supplementary material online, *Figure S2A* and *B*). Together, these results show that the functional decline of H19 during aging contributes to a reduction in endothelial cell function.

3.3 H19 counteracts inflammatory activation

Having demonstrated that H19 is required for proper endothelial cell function, we next aimed to analyse its role in vascular inflammation.

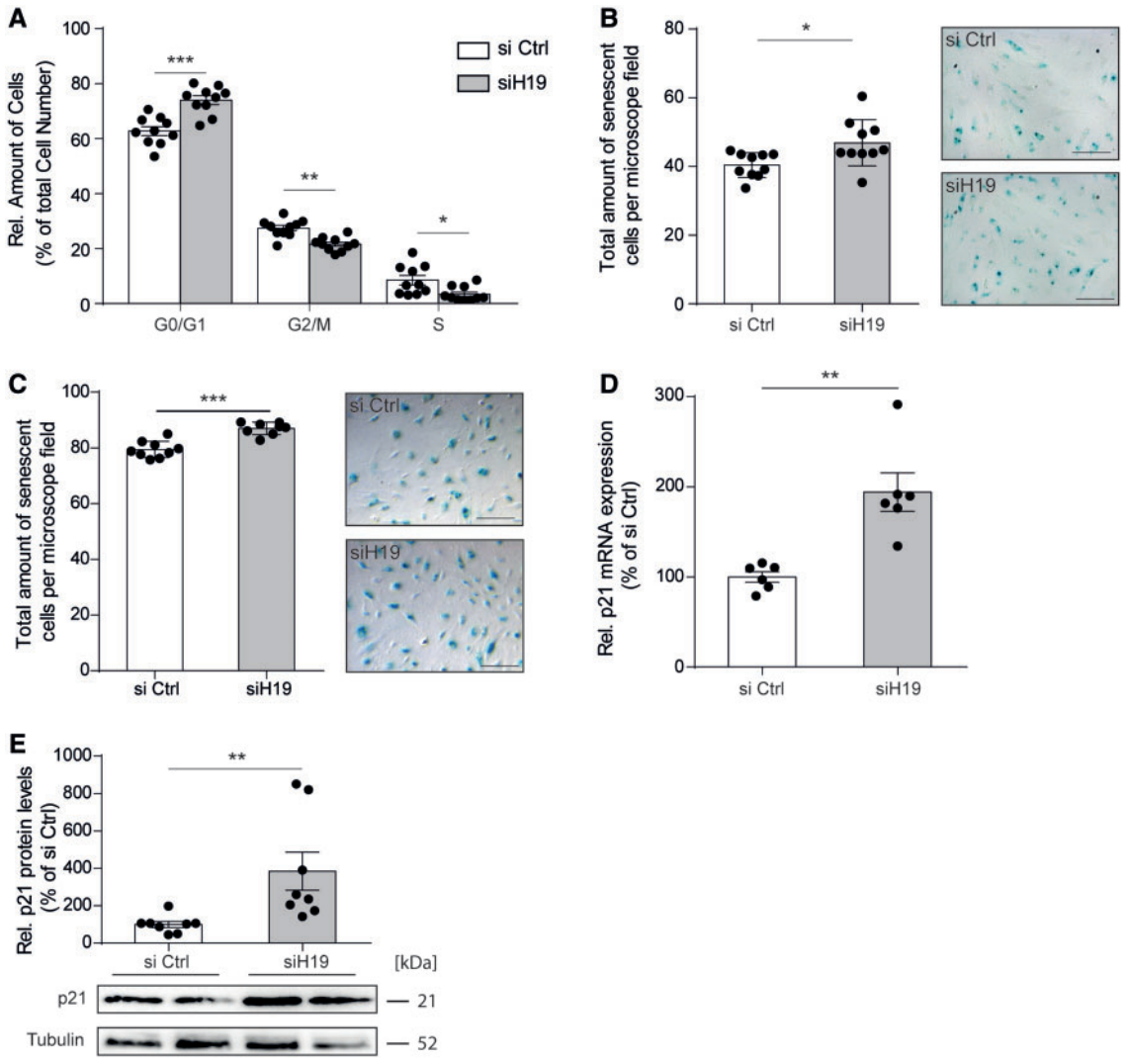

Figure 2 Depletion of H19 promotes senescence in endothelial cells. (*A*) A BrdU flow cytometry assay was performed to analyse EC proliferation upon H19 depletion 48 h after transfection in HUVECs. Results are represented as mean ± SEM from $n = 10$ biological replicates per group. Unpaired *t*-test was used to determine statistical significance. (*B*/*C*) The amount of senescent HUVECs (*B*) and hCoAECs (C) was analysed by staining for senescence-associated β-Galactosidase upon H19 depletion 48 h after transfection. The scale bar denotes 100 µm. Results are represented as mean ± SEM from $n = 10$ or $n = 9$ biological replicates per group, respectively. Unpaired *t*-test was used to determine statistical significance. (*D*/*E*) p21 (CDKN1A) expression upon H19 depletion by siRNAs in HUVECs was analysed on the mRNA level by qRT-PCR (*D*) and on the protein level by immunoblotting (*E*) 48 h after transfection. Results are represented as mean ± SEM from $n = 8$ biological replicates per group. Unpaired *t*-test was used to determine statistical significance; $^{*}P < 0.05$, $^{**}P < 0.01$, and $^{***}P < 0.001$.

Vascular inflammation is characterized by the expression of adhesion molecules and subsequent monocyte infiltration into the underlying tissue.[9] Interestingly, the depletion of H19 in HUVECs increased the expression of the adhesion molecules ICAM-1 and VCAM-1 and their presentation on the cell surface (*Figure 4A* and *B*). Consequently, adhesion of monocytes to HUVECs was enhanced upon H19 depletion *in vitro* and blockage of VCAM-1 with an antibody abolished monocyte adhesion (*Figure 4C* and Supplementary material online, *Figure S2C*). To assess whether H19 plays a role in leucocyte extravasation *in vivo*, the inflammatory activation in the ischaemic legs of $H19^{iEC\text{-}KO}$ mice after hindlimb ischaemia surgery was analysed by staining for $CD45^{+}$ cells. $H19^{iEC\text{-}KO}$ mice showed an increase in leucocyte infiltration into the tissue compared to Ctrl littermates (*Figure 4D*). Furthermore, the regulation of H19 expression under inflammatory activation of ECs was analysed and H19 was downregulated in a time-dependent manner upon stimulation with tumor necrosis factor α (*Figure 4E*). These results indicate that the reduced expression of H19 with age induces inflammatory activation of ECs, which leads to leucocyte infiltration into the underlying tissue. Moreover, inflammatory activation also represses H19 expression. These findings demonstrate that H19 negatively regulates the well described increase in inflammatory activation in aging.

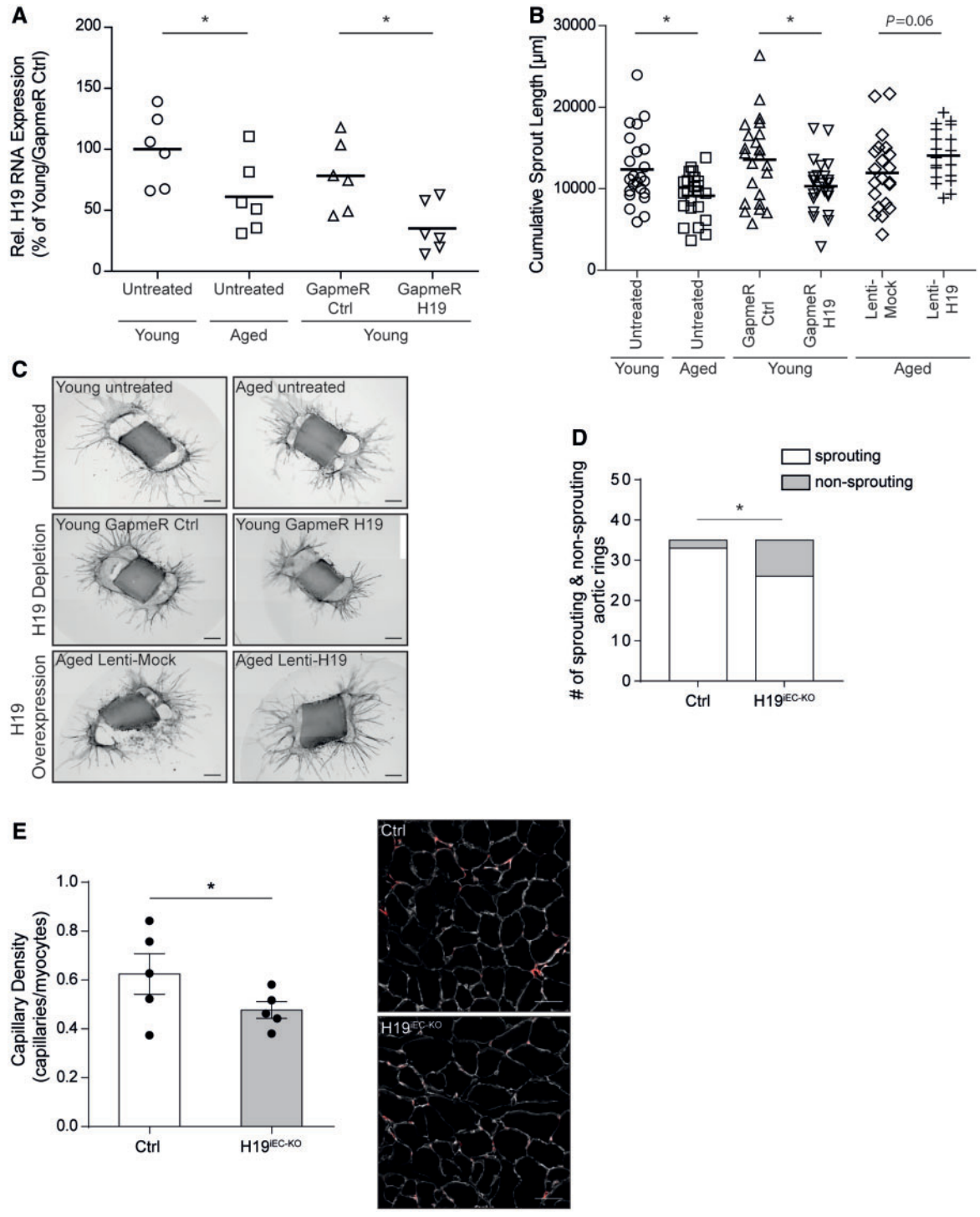

Figure 3 The loss of H19 reduces angiogenesis *in vivo* and *ex vivo*. (*A*) The expression of H19 in aortas of untreated aged (20 months) and young (2 months) mice and in the aortas of young mice upon transfection with LNA Ctrl or LNA H19 was analysed. Results are represented as mean ± SEM from six mice per group. Unpaired *t*-test was used to determine statistical significance. (*B*/*C*) The cumulative sprout length from aortic rings of differentially treated aged and young mice was analysed. ECs were stained with Isolectin B4 and pictures from immunofluorescence microscopy analysis are represented inverted in *C*, and the scale bar denotes 500 µm. Results are represented as mean ± SEM from six mice per group. Unpaired *t*-test was used to determine statistical significance, 3–5 aortic rings per mouse were analysed. Each icon represents an individual aortic ring. (*D*) The amount of sprouting and non-sprouting aortic rings per group was analysed. The χ^2 test was used to compare groups. (*E*) The capillary density in the soleus muscle of endothelial-specific inducible $H19^{iEC\text{-}KO}$ mice and Ctrl littermates was analysed 21 days after hindlimb ischaemia surgery. Endothelial cells are displayed in red, cell membranes are displayed in white. The scale bar denotes 50 µm. Results are represented as mean ± SEM from five mice per group. Unpaired *t*-test was used to determine statistical significance; $^*P < 0.05$ and n.s. = not significant.

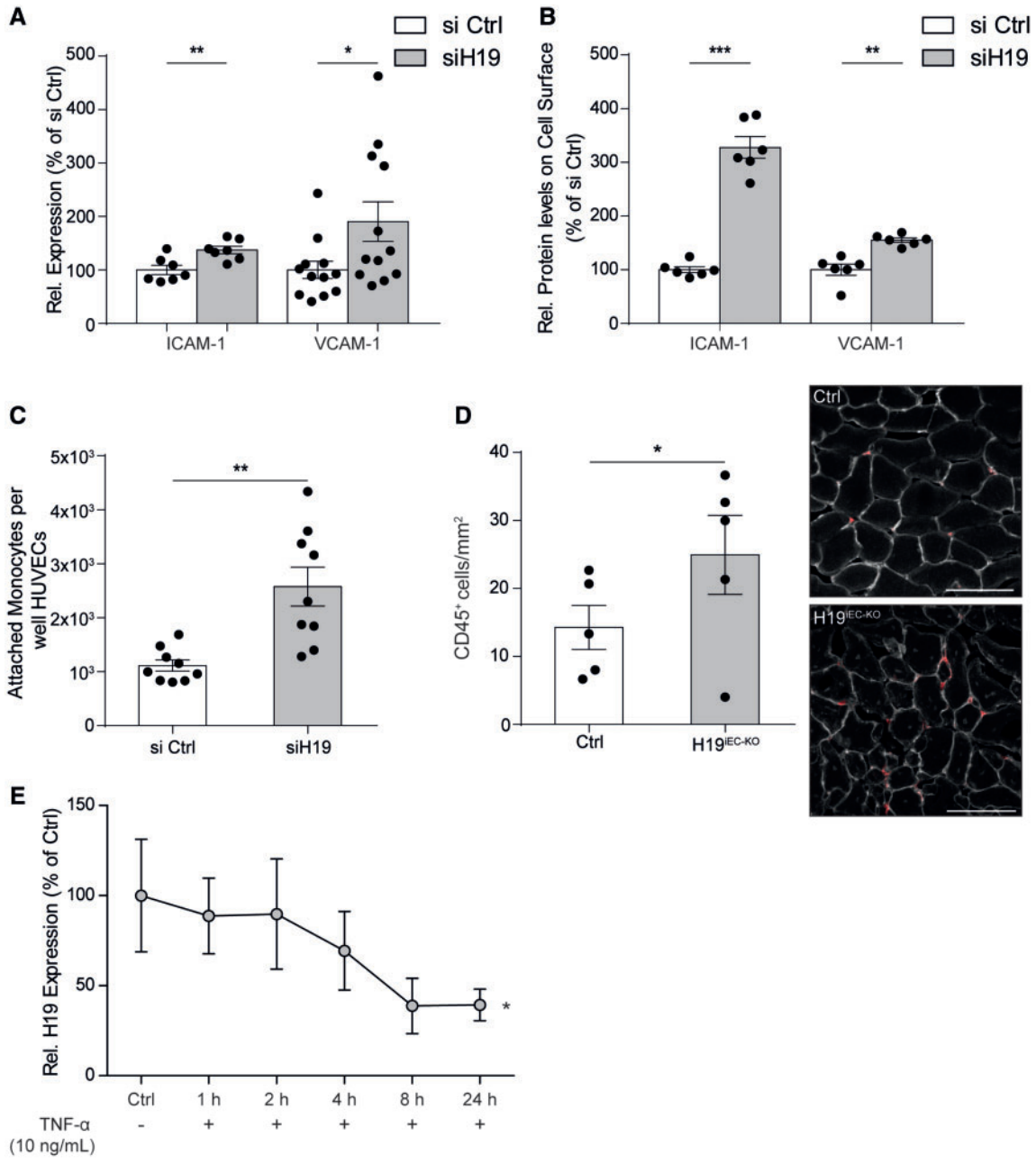

Figure 4 Depletion of H19 facilitates inflammatory activation of ECs. (*A*) The expression of ICAM-1 and VCAM-1 upon H19 depletion in unstimulated HUVECs was analysed by qRT-PCR 48 h after transfection. Results are represented as mean ± SEM from $n = 7$ and $n = 12$ biological replicates per group. Unpaired *t*-test (ICAM-1) and the Mann–Whitney test (VCAM-1) were used to determine statistical significance. (*B*) The cell surface abundance of ICAM-1 and VCAM-1 on HUVECs was analysed by flow cytometry 48 h after siRNA-mediated depletion of H19 and 16 h after stimulation with 100 ng/mL IL-6 and sIL6-Rα. Results are represented as mean ± SEM from $n = 6$ biological replicates per group. Unpaired *t*-test was used to determine statistical significance. (*C*) Adhesion of monocytes to HUVECs was measured upon siRNA-mediated depletion of H19 and stimulation with 100 ng/mL IL-6 and sIL6-Rα for 16 h in HUVECs, 48 h after transfection. Results are represented as mean ± SEM from $n = 9$ biological replicates per group. Unpaired *t*-test was used to determine statistical significance. (*D*) The number of $CD45^+$ cells in the soleus muscle of endothelial-specific inducible $H19^{iEC\text{-}KO}$ mice and Ctrl littermates was analysed 21 days after hindlimb ischaemia surgery. $CD45^+$ cells are displayed in red, cell membranes are displayed in white. The scale bar denotes 100 µm. Results are represented as mean ± SEM from five mice per group. Unpaired *t*-test was used to determine statistical significance. (*E*) H19 expression in wild-type HUVECs was analysed by qRT-PCR at 1 h, 2 h, 4 h, 8 h, and 24 h after stimulation with tumor necrosis factor α. Results are represented as mean ± SEM from $n = 5$ to $n = 7$ biological replicates per group. A post-test for linear trend was used to determine statistical significance.; $^*P < 0.05$, $^{**}P < 0.01$, and $^{***}P < 0.001$.

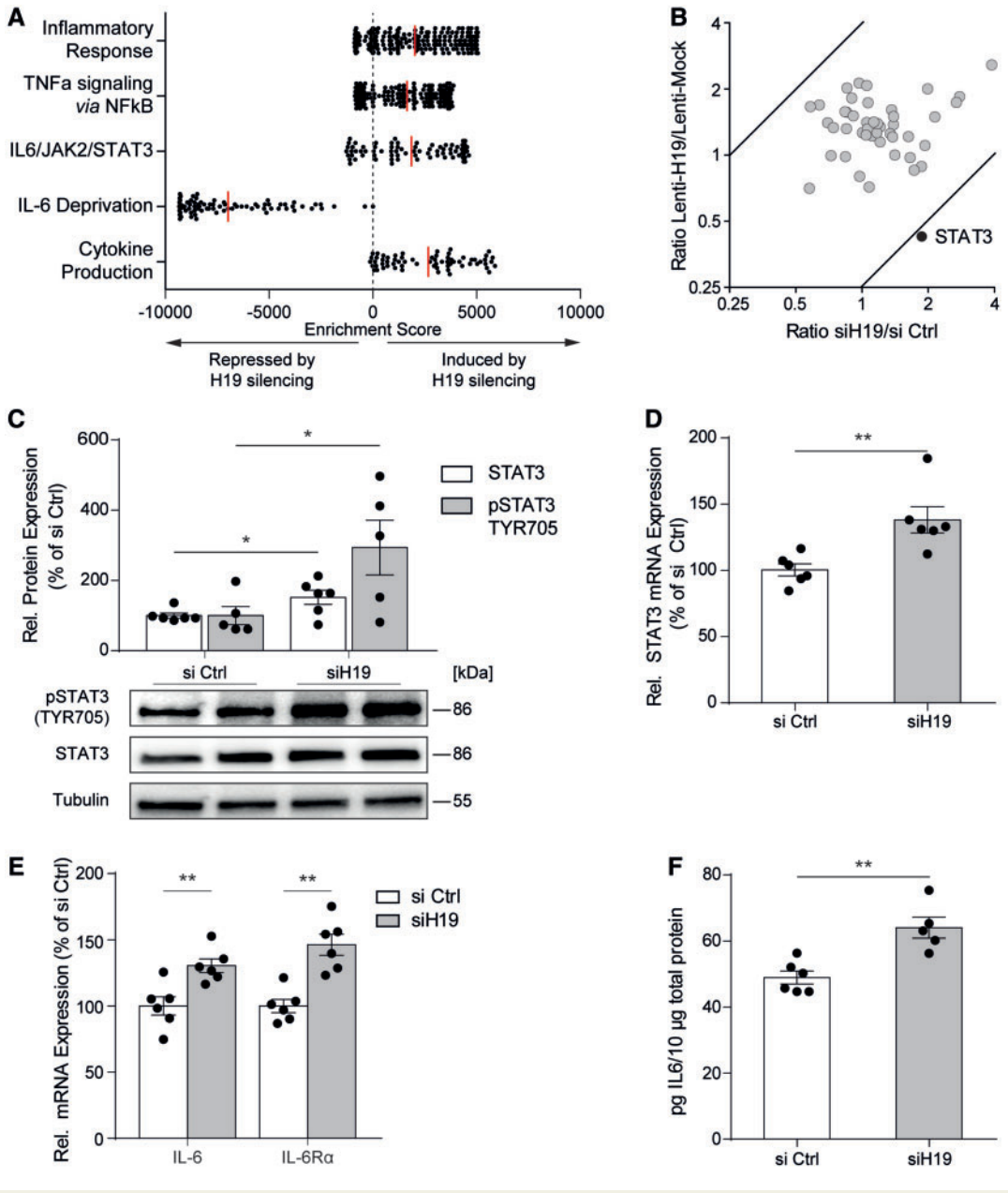

Figure 5 H19 suppresses the activation of STAT3. (*A*) An unbiased microarray screen of HUVECs after siRNA-mediated H19 depletion was analysed for differentially regulated pathways, using Gene Set Enrichment Analysis. Enrichment scores of the indicated pathways are plotted on the *x* axis. (*B*) A high throughput transcription factor activity reporter luciferase assay upon siRNA-mediated depletion or lentiviral overexpression of H19 in HeLa cells was performed 48 h after transfection or 7 days after transduction, respectively. Depicted are ratios for activity of 45 transcription factors in siH19/si Ctrl treated cells (*x* axis) and Lenti-H19/Lenti-Mock treated cells (*y* axis) 24 h after transfection with the reporter constructs. STAT3 reporter activity is highlighted in black. (*C*) STAT3 total levels and levels of phosphorylated STAT3 at TYR705 were analysed by western blot upon H19 depletion 48 h after transfection in HUVECs. Results are represented as mean ± SEM from $n = 6$ biological replicates per group. Unpaired *t*-test was used to determine statistical significance. (*D*) The expression of STAT3 mRNA was analysed upon silencing of H19 by qRT-PCR 48 h after transfection in HUVECs. Results are represented as mean ± SEM from $n = 6$ biological replicates per group. Unpaired *t*-test was used to determine statistical significance. (*E*) The mRNA expression of IL-6 and IL-6Rα in HUVECs was analysed after H19 depletion by qPCR 48 h after transfection. Results are represented as mean ± SEM from $n = 6$ biological replicates per group. Unpaired *t*-test was used to determine statistical significance. (*F*) The concentration of intracellular IL-6 in HUVECs was analysed upon H19 depletion in an ELISA 48 h after transfection. Results are represented as mean ± SEM from $n = 5$ biological replicates per group. Unpaired *t*-test was used to determine statistical significance; $^{*}P < 0.05$ and $^{**}P < 0.01$.

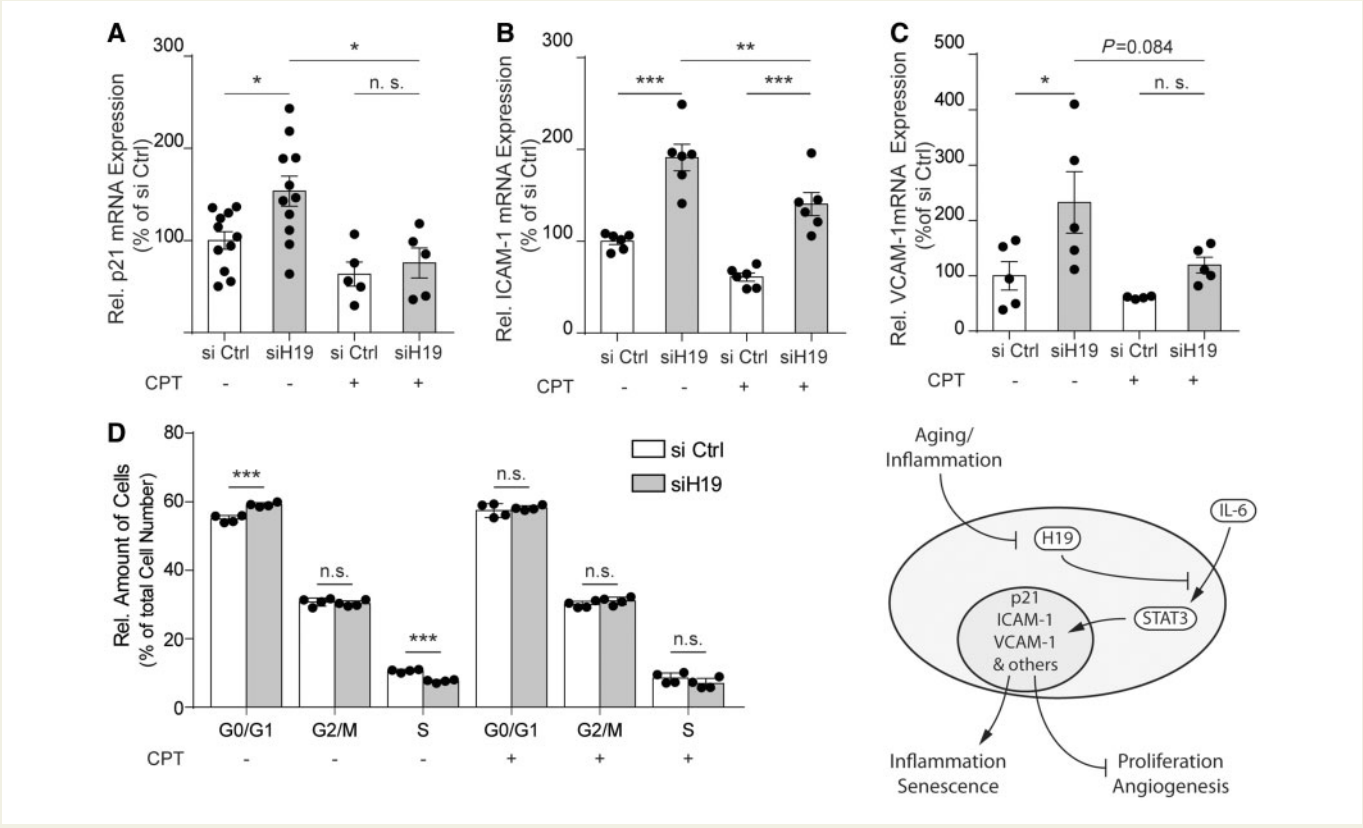

Figure 6 Inhibition of STAT3 activation partially rescues the effects of H19 silencing. (*A*) Expression of p21 was analysed upon depletion of H19 and inhibition of STAT3 activation with CPT in HUVECs 48 h after transfection. Cells were stimulated with 100 ng/μL IL-6 and sIL-6Rα for 16 h and with 20 μM CPT for 17 h before the start of the experiment. Results are represented as mean ± SEM from $n = 11$ and $n = 5$ biological replicates per group respectively. One-way ANOVA followed by Tukey's post-test was used to determine statistical significance. (*B*) Expression of ICAM-1 was analysed upon depletion of H19 and inhibition of STAT3 activation with CPT in HUVECs 48 h after transfection. Cells were stimulated with 100 ng/μL IL-6 and sIL-6Rα for 16 h and with 20 μM CPT for 17 h before the start of the experiment. Results are represented as mean ± SEM from $n = 6$ biological replicates per group. One-way ANOVA followed by Tukey's post-test was used to determine statistical significance. (*C*) Expression of VCAM-1 was analysed upon depletion of H19 and inhibition of STAT3 activation with CPT in HUVECs 48 h after transfection. Cells were stimulated with 100 ng/μL IL-6 and sIL-6Rα for 16 h and with 20 μM CPT for 17 h before the start of the experiment. Results are represented as mean ± SEM from $n = 5$ biological replicates per group. One-way ANOVA followed by Tukey's post-test was used to determine statistical significance. (*D*) A BrdU flow cytometry assay was performed after depletion of H19 and inhibition of STAT3 activation by CPT treatment 48 h after transfection in HUVECs. Cells were stimulated with 100 ng/μL IL-6 and sIL-6Rα for 16 h and with 20 μM CPT for 17 h before the start of the experiment. Results are represented as mean ± SEM from $n = 4$ biological replicates per group. Unpaired *t*-test was used to determine statistical significance. (*E*) Overview of H19 functions in ECs; $^*P < 0.05$, $^{**}P < 0.01$, $^{***}P < 0.001$, and n.s. = not significant.

3.4 H19 regulates STAT3 signalling in endothelial cells

To analyse the mechanism by which H19 regulates endothelial cell function, an unbiased microarray analysis upon siRNA-mediated depletion of H19 was performed and gene set enrichment analysis[57] identified many proliferation- and inflammation-related pathways. Among those were several pathways associated with IL-6/STAT3 signalling (*Figure 5A* and Supplementary material online, *Figure S2D*). Importantly, an unbiased luciferase transcription factor activity reporter assay, containing reporters for 45 transcription factors, identified STAT3 as being the most differentially active upon H19 depletion and overexpression (*Figure 5B* and Supplementary material online, *Figure S2E*). STAT3 activity was increased upon H19 depletion and decreased upon H19 overexpression, indicating that H19 inhibits STAT3 signalling. Since IL-6/STAT3 signalling induces STAT3 phosphorylation, we first assessed whether H19 regulates STAT3 phosphorylation. The phosphorylation of STAT3 at tyrosine 705 was strongly increased upon H19 depletion (*Figure 5C*). To a minor extent, the expression levels of STAT3 on mRNA and protein level were also increased after H19 silencing (*Figure 5C* and *D*). Consistently, the expression of IL-6 and IL-6Rα was induced upon H19 depletion, likely as a downstream effect of the increased STAT3 activity (*Figure 5E* and *F*). These results show that H19 is involved in the regulation of inflammatory processes and its depletion favours a pro-inflammatory environment, characterized by IL-6 signalling and STAT3 activation.

3.5 H19 regulates proliferation and inflammatory activation via STAT3 inhibition

STAT3 is known to regulate p21 and ICAM-1. We therefore determined whether H19-mediated inhibition of STAT3 signalling contributes to regulation of proliferation and inflammatory activation by H19. The

inhibition of STAT3 with CPT abolished the H19 depletion-mediated induction of p21 (*Figure 6A*). Furthermore, the induction of ICAM-1 and VCAM-1 after H19 depletion was attenuated by STAT3 inhibition as well (*Figure 6B* and *C*). Interestingly, induction of p16 mRNA expression was not affected by STAT3 inhibition (Supplementary material online, *Figure S2D*). Moreover, inhibition of STAT3 activation also abolished the effect of H19 depletion on HUVEC proliferation (*Figure 6D*). These results show that the anti-inflammatory and proliferative effects mediated by H19 in ECs are at least partially due to inhibition of STAT3 activation.

4. Discussion

Our results demonstrate that H19 is an essential regulator of endothelial senescence and inflammatory activation and that H19 expression is diminished during aging, mainly in endothelial cells. Loss of H19 is accompanied by impaired angiogenic sprouting and an increase in infiltration of immune cells. Mechanistically, H19 inhibits the phosphorylation of STAT3 at TYR705 and thus the expression of STAT3 target genes (*Figure 6E*).

H19 expression is repressed with aging *in vivo* in the endothelium and under inflammatory activation *in vitro* (*Figures 1A, B* and *4E*). Under basal conditions, H19 is expressed in luminal endothelium *in vivo*, but repressed upon atherosclerotic plaque formation (*Figure 1C* and *D*). How H19 expression is regulated during aging is still elusive but bioinformatic analysis revealed binding sites for members of the KLF transcription factor family in the H19 promoter region (Supplementary material online, *Figure S3A*). KLF2 was previously shown to possess atheroprotective effects,[54] and we show that lentiviral overexpression of KLF2 induces the expression of H19 (Supplementary material online, *Figure S3B*), showing a potential role of KLF2 in controlling H19 expression.

Aging is known to have multiple synergistic effects on the endothelium. These hallmarks of aging include a decrease of proliferative capacity and an increase in inflammatory activation.[58] Our data show that H19 regulates at least these two hallmarks of aging. A decline of endothelial H19 expression with aging therefore, likely contributes to endothelial senescence and inflammatory activation. Senescent cells are known to secrete inflammatory cytokines like IL-6.[10–12] Depletion of H19 in HUVECs led to increased expression of IL-6 and subsequently to increased inflammatory activation, indicating that the loss of H19 with age might promote inflammatory activation *in vivo* (*Figure 5E* and *F*). Cells within atherosclerotic plaques show markers of inflammatory activation and H19 is less expressed in these specimens (*Figure 1C*). Furthermore, regions of atherosclerotic plaques also show enhanced senescence[17] and the increase in senescence upon H19 depletion in endothelial cells indicates H19 might play a role in this process (*Figure 2B* and *C*). Indeed in our hindlimb ischaemia model of endothelial cell function, angiogenesis is impaired and inflammation is increased after endothelial-specific deletion of H19. Interestingly, these two processes counteract in terms of perfusion of the hindlimb, where impaired angiogenesis decreases perfusion, but inflammation increases perfusion, resulting in a net perfusion that is not affected (Supplementary material online, *Figure S3C*). Since declined tissue perfusion is a clinical feature of aging,[59] these data indicate that other H19-independent processes also control perfusion or that non-endothelial-intrinsic mechanisms play a role. Interestingly, EC-specific H19 depletion was sufficient to increase systolic blood pressure in mice, supporting our hypothesis that loss of endothelial H19 has detrimental effects on the vasculature.

Mechanistically, our data show that H19 controls proliferation and inflammation *via* STAT3 inhibition. Interestingly, STAT3 depletion in aged mice accelerated tissue repair, while this effect was absent in young mice.[23] At which stage H19 inhibits STAT3 phosphorylation is currently unclear. However, inhibition of STAT3 activation was sufficient to abolish the induction of p21 and VCAM-1 upon pharmacological inhibition of H19. ICAM-1 was still induced upon inhibition of STAT3 activation and depletion of H19, but significantly less than with active STAT3, suggesting that H19 regulates ICAM-1 at least partially *via* STAT3. H19 was shown to act as a sponge for several microRNAs.[60–62] However, bioinformatic analysis of publicly available Argonaute HITS-CLIP data did not show an association of H19 with miRNAs in bone marrow ECs[63] (Supplementary material online, *Figure S3D*). H19 is predominantly located in the cytoplasm of HUVECs (Supplementary material online, *Figure S3E*) and RIP experiments showed that H19 was not associated to histone H3, H3K27me3 or H3K9me3 (Supplementary material online, *Figure S3F*), excluding epigenetic regulation of gene expression. Another published feature of H19 is that it can act as a precursor molecule for miR-675, which was shown to promote skeletal muscle differentiation and regeneration.[37] However, in our experiments, depletion of H19 does not reduce miR-675 expression in HUVECs (Supplementary material online, *Figure S3G*), indicating that miR-675 likely does not contribute to H19 function in ECs.

In summary, the lncRNA H19 is repressed during aging and controls endothelial cell senescence, proliferation, inflammatory activation and angiogenic sprouting by inhibiting STAT3 activation. These results implicate H19 as a key mediator of endothelial cell function and identify H19 as a potential therapeutic target to augment endothelial cell function in aged individuals.

Supplementary material

Supplementary material is available at *Cardiovascular Research* online.

Acknowledgements

We thank Andrea Knau, Marion Muhly-Reinholz, and Denise Berghäuser for technical support and Martin Maeng Bjorklund and Jacob Fog Bentzon for providing crucial experimental reagents.

Conflict of interest: none declared.

Funding

This work was supported by the Deutsche Forschungsgemeinschaft [SFB834 to R.A.B. and S.D.] and the European Research Council ['NOVA' to R.A.B. and 'Angiolnc' to S.D.]. The BiKE study was conducted with support from the Swedish Heart and Lung Foundation, the Swedish Research Council [K2009-65X-2233-01-3, K2013-65X-06816-30-4 and 349-2007-8703], Uppdrag Besegra Stroke [P581/2011-123], the Strategic Cardiovascular Programs of Karolinska Institutet and Stockholm County Council, the Stockholm County Council [ALF2011-0260 and ALF-2011-0279], and the Foundation for Strategic Research and the European Commission [CarTarDis, AtheroRemo, VIA, and AtheroFlux projects].

References

1. Go AS, Mozaffarian D, Roger VL, Benjamin EJ, Berry JD, Borden WB, Bravata DM, Dai S, Ford ES, Fox CS, Franco S, Fullerton HJ, Gillespie C, Hailpern SM, Heit JA, Howard VJ, Huffman MD, Kissela BM, Kittner SJ, Lackland DT, Lichtman JH, Lisabeth

LD, Magid D, Marcus GM, Marelli A, Matchar DB, McGuire DK, Mohler ER, Moy CS, Mussolino ME, Nichol G, Paynter NP, Schreiner PJ, Sorlie PD, Stein J, Turan TN, Virani SS, Wong ND, Woo D, Turner MB. Heart disease and stroke statistics–2013 update: a report from the American Heart Association. *Circulation* 2013;**127**: e6–e245.
2. Lakatta EG, Levy D. Arterial and cardiac aging: major shareholders in cardiovascular disease enterprises: part I: aging arteries: a 'set up' for vascular disease. *Circulation* 2003;**107**:139–146.
3. Rodier F, Campisi J. Four faces of cellular senescence. *J Cell Biol* 2011;**192**:547–556.
4. Campisi J. Aging, cellular senescence, and cancer. *Annu Rev Physiol* 2013;**75**: 685–705.
5. Sharpless NE, Sherr CJ. Forging a signature of *in vivo* senescence. *Nat Rev Cancer* 2015;**15**:397–408.
6. van Deursen JM. The role of senescent cells in ageing. *Nature* 2014;**509**:439–446.
7. Vasa M, Breitschopf K, Zeiher AM, Dimmeler S. Nitric oxide activates telomerase and delays endothelial cell senescence. *Circ Res* 2000;**87**:540–542.
8. Matsushita H, Chang E, Glassford AJ, Cooke JP, Chiu CP, Tsao PS. eNOS activity is reduced in senescent human endothelial cells: preservation by hTERT immortalization. *Circ Res* 2001;**89**:793–798.
9. Gimbrone MA, Topper JN, Nagel T, Anderson KR, Garcia-Cardeña G. Endothelial dysfunction, hemodynamic forces, and atherogenesis. *Ann N Y Acad Sci* 2006;**902**: 230–239; discussion 239–40.
10. Coppé J-P, Desprez P-Y, Krtolica A, Campisi J. The senescence-associated secretory phenotype: the dark side of tumor suppression. *Annu Rev Pathol Mech Dis* 2010;**5**: 99–118.
11. Coppé J-P, Patil CK, Rodier F, Sun Y, Muñoz DP, Goldstein J, Nelson PS, Desprez P-Y, Campisi J. Senescence-associated secretory phenotypes reveal cell-nonautonomous functions of oncogenic RAS and the p53 tumor suppressor. *PLoS Biol* 2008;**6**:2853–68.
12. Kuilman T, Michaloglou C, Vredeveld LCW, Douma S, Doorn R, van Desmet CJ, Aarden LA, Mooi WJ, Peeper DS. Oncogene-induced senescence relayed by an interleukin-dependent inflammatory network. *Cell* 2008;**133**:1019–1031.
13. Bernal GM, Wahlstrom JS, Crawley CD, Cahill KE, Pytel P, Liang H, Kang S, Weichselbaum RR, Yamini B. Loss of *Nfkb1* leads to early onset aging. *Aging (Albany NY)* 2014;**6**:931–943.
14. Baker DJ, Childs BG, Durik M, Wijers ME, Sieben CJ, Zhong J, A. Saltness R, Jeganathan KB, Verzosa GC, Pezeshki A, Khazaie K, Miller JD, van Deursen JM. Naturally occurring p16(Ink4a)-positive cells shorten healthy lifespan. *Nature* 2016; **530**:184–189.
15. Le Couteur DG, Lakatta EG. A vascular theory of aging. *J Gerontol A Biol Sci Med Sci* 2010;**65**:1025–1027.
16. Das A, Huang GX, Bonkowski MS, Longchamp A, Li C, Schultz MB, Kim L-J, Osborne B, Joshi S, Lu Y, Treviño-Villarreal JH, Kang M-J, Hung T, Lee B, Williams EO, Igarashi M, Mitchell JR, Wu LE, Turner N, Arany Z, Guarente L, Sinclair DA. Impairment of an endothelial NAD^+-H_2S signaling network is a reversible cause of vascular aging. *Cell* 2018;**173**:74–89.e20.
17. Minamino T, Miyauchi H, Yoshida T, Ishida Y, Yoshida H, Komuro I. Endothelial cell senescence in human atherosclerosis: role of telomere in endothelial dysfunction. *Circulation* 2002;**105**:1541–1544.
18. Wang J, Uryga AK, Reinhold J, Figg N, Baker L, Finigan A, Gray K, Kumar S, Clarke M, Bennett M. Vascular smooth muscle cell senescence promotes atherosclerosis and features of plaque vulnerability. *Circulation* 2015;**132**:1909–1919.
19. Matthews C, Gorenne I, Scott S, Figg N, Kirkpatrick P, Ritchie A, Goddard M, Bennett M. Vascular smooth muscle cells undergo telomere-based senescence in human atherosclerosis: effects of telomerase and oxidative stress. *Circ Res* 2006;**99**: 156–164.
20. Holdt LM, Sass K, Gäbel G, Bergert H, Thiery J, Teupser D. Expression of Chr9p21 genes *CDKN2B* (*p15INK4b*), *CDKN2A* (*p16INK4a*, *p14ARF*) and MTAP in human atherosclerotic plaque. *Atherosclerosis* 2011;**214**:264–270.
21. Kishimoto T. Interleukin-6: discovery of a pleiotropic cytokine. *Arthritis Res Ther* 2006; **8** (Suppl. 2):S2.
22. Hartman J, Frishman WH. Inflammation and atherosclerosis: a review of the role of interleukin-6 in the development of atherosclerosis and the potential for targeted drug therapy. *Cardiol Rev* 2014;**22**:147–151.
23. Tierney MT, Aydogdu T, Sala D, Malecova B, Gatto S, Puri PL, Latella L, Sacco A. STAT3 signaling controls satellite cell expansion and skeletal muscle repair. *Nat Med* 2014;**20**:1182–1186.
24. Liu R, Wang L, Chen G, Katoh H, Chen C, Liu Y, Zheng P. *FOXP3* up-regulates p21 expression by site-specific inhibition of histone deacetylase 2/4 association to the locus. *Cancer Res* 2009;**69**:2252–2259.
25. Zorn E, Nelson EA, Mohseni M, Porcheray F, Kim H, Litsa D, Bellucci R, Raderschall E, Canning C, Soiffer RJ, Frank DA, Ritz J. IL-2 regulates *FOXP3* expression in human $CD4^+CD25^+$ regulatory T cells through a STAT-dependent mechanism and induces the expansion of these cells in vivo. *Blood* 2006;**108**:1571–1579.
26. Schuringa JJ, Timmer H, Luttickhuizen D, Vellenga E, Kruijer W. c-Jun and c-Fos cooperate with STAT3 in IL-6-induced transactivation of the IL-6 respone element (IRE). *Cytokine* 2001;**14**:78–87.
27. Wung BS, Ni CW, Wang DL. ICAM-1 induction by TNFalpha and IL-6 is mediated by distinct pathways via Rac in endothelial cells. *J Biomed Sci* 2005;**12**:91–101.
28. Durant L, Watford WT, Ramos HL, Laurence A, Vahedi G, Wei L, Takahashi H, Sun H-W, Kanno Y, Powrie F, O'Shea JJ. Diverse targets of the transcription factor STAT3 contribute to T cell pathogenicity and homeostasis. *Immunity* 2010;**32**: 605–615.
29. Yoon S, Woo SU, Kang JH, Kim K, Shin H-J, Gwak H-S, Park S, Chwae Y-J. NF-κB and STAT3 cooperatively induce IL6 in starved cancer cells. *Oncogene* 2012;**31**: 3467–3481.
30. Volders P-J, Verheggen K, Menschaert G, Vandepoele K, Martens L, Vandesompele J, Mestdagh P. An update on LNCipedia: a database for annotated human lncRNA sequences. *Nucleic Acids Res* 2015;**43**:4363–4380.
31. Uchida S, Dimmeler S. Long noncoding RNAs in cardiovascular diseases. *Circ Res* 2015;**116**:737–750.
32. Michalik KM, You X, Manavski Y, Doddaballapur A, Zörnig M, Braun T, John D, Ponomareva Y, Chen W, Uchida S, Boon RA, Dimmeler S. Long noncoding RNA MALAT1 regulates endothelial cell function and vessel growth. *Circ Res* 2014;**114**: 1389–1397.
33. Pachnis V, Belayew A, Tilghman SM. Locus unlinked to alpha-fetoprotein under the control of the murine raf and Rif genes. *Proc Natl Acad Sci U S A* 1984;**81**:5523–5527.
34. Brannan CI, Dees EC, Ingram RS, Tilghman SM. The product of the H19 gene may function as an RNA. *Mol Cell Biol* 1990;**10**:28–36.
35. Leibovitch MP, Nguyen VC, Gross MS, Solhonne B, Leibovitch SA, Bernheim A. The human ASM (adult skeletal muscle) gene: expression and chromosomal assignment to 11p15. *Biochem Biophys Res Commun* 1991;**180**:1241–1250.
36. Ayesh S, Matouk I, Schneider T, Ohana P, Laster M, Al-Sharef W, De-Groot N, Hochberg A. Possible physiological role of H19 RNA. *Mol Carcinog* 2002;**35**:63–74.
37. Dey BK, Pfeifer K, Dutta A. The H19 long noncoding RNA gives rise to microRNAs miR-675-3p and miR-675-5p to promote skeletal muscle differentiation and regeneration. *Genes Dev* 2014;**28**:491–501.
38. Bartolomei MS, Zemel S, Tilghman SM. Parental imprinting of the mouse H19 gene. *Nature* 1991;**351**:153–155.
39. Voellenkle C, Garcia-Manteiga JM, Pedrotti S, Perfetti A, Toma I, De Silva D, Da Maimone B, Greco S, Fasanaro P, Creo P, Zaccagnini G, Gaetano C, Martelli F. Implication of Long noncoding RNAs in the endothelial cell response to hypoxia revealed by RNA-sequencing. *Sci Rep* 2016;**6**:24141.
40. Deng Y, Yang Z, Terry T, Pan S, Woodside DG, Wang J, Ruan K, Willerson JT, Dixon RAF, Liu Q. Prostacyclin-producing human mesenchymal cells target H19 lncRNA to augment endogenous progenitor function in hindlimb ischaemia. *Nat Commun* 2016;**7**:11276.
41. Hadji F, Boulanger M-C, Guay S-P, Gaudreault N, Amellah S, Mkannez G, Bouchareb R, Tremblay-Marchand J, Nsaibia MJ, Guauque-Olarte S, Pibarot P, Bouchard L, Bossé Y, Mathieu P. Altered DNA methylation of long non-coding RNA *H19* in calcific aortic valve disease promotes mineralization by silencing *NOTCH1*. *Circulation* 2016;**134**:1848–1862.
42. Naylor AR, Cuffe RL, Rothwell PM, Bell PRF, Ura M, Sakata R, Naylor C, Goldenkrantz R, Huston J, Parsonnet V, Zogno M, Giulini S, Crawford B, Glassman L, Baumann F, Spencer F. A systematic review of outcomes following staged and synchronous carotid endarterectomy and coronary artery bypass. *Eur J Vasc Endovasc Surg* 2003;**25**:380–389.
43. Halliday A, Harrison M, Hayter E, Kong X, Mansfield A, Marro J, Pan H, Peto R, Potter J, Rahimi K, Rau A, Robertson S, Streifler J, Thomas D; Asymptomatic Carotid Surgery Trial (ACST) Collaborative Group. 10-year stroke prevention after successful carotid endarterectomy for asymptomatic stenosis (ACST-1): a multicentre randomised trial. *Lancet* 2010;**376**:1074–1084.
44. Perisic Matic L, Rykaczewska U, Razuvaev A, Sabater-Lleal M, Lengquist M, Miller CL, Ericsson I, Röhl S, Kronqvist M, Aldi S, Magné J, Paloschi V, Vesterlund M, Li Y, Jin H, Diez MG, Roy J, Baldassarre D, Veglia F, Humphries SE, de Faire U, Tremoli E, Odeberg J, Vukojević V, Lehtiö J, Maegdefessel L, Ehrenborg E, Paulsson-Berne G, Hansson GK, Lindeman JHN, Eriksson P, Quertermous T, Hamsten A, Hedin U. Phenotypic modulation of smooth muscle cells in atherosclerosis is associated with downregulation of LMOD1, SYNPO2, PDLIM7, PLN, and SYNM. *Arterioscler Thromb Vasc Biol* 2016;**36**:1947–1961.
45. Perisic L, Aldi S, Sun Y, Folkersen L, Razuvaev A, Roy J, Lengquist M, Ökesson S, Wheelock CE, Maegdefessel L, Gabrielsen A, Odeberg J, Hansson GK, Paulsson-Berne G, Hedin U. Gene expression signatures, pathways and networks in carotid atherosclerosis. *J Intern Med* 2016;**279**:293–308.
46. Pelisek J, Wendorff H, Wendorff C, Kuehnl A, Eckstein H-H. Age-associated changes in human carotid atherosclerotic plaques. *Ann Med* 2016;**48**:541–551.
47. Stary HC, Chandler AB, Dinsmore RE, Fuster V, Glagov S, Insull W, Rosenfeld ME, Schwartz CJ, Wagner WD, Wissler RW. A definition of advanced types of atherosclerotic lesions and a histological classification of atherosclerosis. A report from the Committee on Vascular Lesions of the Council on Arteriosclerosis, American Heart Association. *Circulation* 1995;**92**:1355–1374.
48. Redgrave JN, Gallagher P, Lovett JK, Rothwell PM. Critical cap thickness and rupture in symptomatic carotid plaques: the Oxford Plaque Study. *Stroke* 2008;**39**: 1722–1729.
49. Hwang H-W, Wentzel EA, Mendell JT. A hexanucleotide element directs microRNA nuclear import. *Science* 2007;**315**:97–100.
50. Dekker RJ, Thienen JV, van Rohlena J, Jager SC, de Elderkamp YW, Seppen J, Vries CJM, de Biessen EAL, Berkel TJC, van Pannekoek H, Horrevoets AJ. Endothelial *KLF2*

links local arterial shear stress levels to the expression of vascular tone-regulating genes. *Am J Pathol* 2005;**167**:609–618.
51. Zufferey R, Nagy D, Mandel RJ, Naldini L, Trono D. Multiply attenuated lentiviral vector achieves efficient gene delivery *in vivo*. *Nat Biotechnol* 1997;**15**:871–875.
52. Boon RA, Iekushi K, Lechner S, Seeger T, Fischer A, Heydt S, Kaluza D, Tréguer K, Carmona G, Bonauer A, Horrevoets AJG, Didier N, Girmatsion Z, Biliczki P, Ehrlich JR, Katus H. A, Müller OJ, Potente M, Zeiher AM, Hermeking H, Dimmeler S. MicroRNA-34a regulates cardiac ageing and function. *Nature* 2013;**495**:107–110.
53. Baker M, Robinson SD, Lechertier T, Barber PR, Tavora B, D'Amico G, Jones DT, Vojnovic B, Hodivala-Dilke K. Use of the mouse aortic ring assay to study angiogenesis. *Nat Protoc* 2011;**7**:89–104.
54. Boon RA, Urbich C, Fischer A, Fontijn RD, Seeger FH, Koyanagi M, Horrevoets AJG, Dimmeler S. Kruppel-like factor 2 improves neovascularization capacity of aged proangiogenic cells. *Eur Heart J* 2011;**32**:371–377.
55. Boon RA, Seeger T, Heydt S, Fischer A, Hergenreider E, Horrevoets AJG, Vinciguerra M, Rosenthal N, Sciacca S, Pilato M, Heijningen P, van Essers J, Brandes RP, Zeiher AM, Dimmeler S. MicroRNA-29 in aortic dilation: implications for aneurysm formation. *Circ Res* 2011;**109**:1115–1119.
56. Ahluwalia A, Jones MK, Szabo S, Tarnawski AS. Aging impairs transcriptional regulation of vascular endothelial growth factor in human microvascular endothelial cells: implications for angiogenesis and cell survival. *J Physiol Pharmacol* 2014;**65**:209–215.
57. Subramanian A, Tamayo P, Mootha VK, Mukherjee S, Ebert BL, Gillette MA, Paulovich A, Pomeroy SL, Golub TR, Lander ES, Mesirov JP. Gene set enrichment analysis: a knowledge-based approach for interpreting genome-wide expression profiles. *Proc Natl Acad Sci U S A* 2005;**102**:15545–15550.
58. López-Otín C, Blasco MA, Partridge L, Serrano M, Kroemer G. The hallmarks of aging. *Cell* 2013;**153**:1194–1217.
59. Park S-Y, Ives SJ, Gifford JR, Andtbacka RHI, Hyngstrom JR, Reese V, Layec G, Bharath LP, Symons JD, Richardson RS. Impact of age on the vasodilatory function of human skeletal muscle feed arteries. *Am J Physiol Heart Circ Physiol* 2016;**310**:H217–H225.
60. Kallen AN, Zhou X-B, Xu J, Qiao C, Ma J, Yan L, Lu L, Liu C, Yi J-S, Zhang H, Min W, Bennett AM, Gregory RI, Ding Y, Huang Y. The imprinted H19 LncRNA antagonizes Let-7 MicroRNAs. *Mol Cell* 2013;**52**:101–112.
61. Imig J, Brunschweiger A, Mmer AB, Uuml Guennewig B, Mittal N, Kishore S, Tsikrika P, Gerber A, Eacute P, Zavolan M, Hall J. miR-CLIP capture of a miRNA targetome uncovers a lincRNA H19-miR-106a interaction. *Nat Chem Biol* 2015;**11**:107–110.
62. Luo M, Li Z, Wang W, Zeng Y, Liu Z, Qiu J. Long non-coding RNA H19 increases bladder cancer metastasis by associating with EZH2 and inhibiting E-cadherin expression. *Cancer Lett* 2013;**333**:213–221.
63. Balakrishnan I, Yang X, Brown J, Ramakrishnan A, Torok-Storb B, Kabos P, Hesselberth JR, Pillai MM. Genome-wide analysis of miRNA-mRNA interactions in marrow stromal cells. *Stem Cells* 2014;**32**:662–673.